ORIGINAL PAPER

A comparative study of microstructural development in the sol–gel derived alumina–mullite nanocomposites using colloidal silica and tetraethyl orthosilicate

A. Sedaghat · E. Taheri-Nassaj · G. D. Soraru · T. Ebadzadeh

Abstract This paper compares the microstructure development of two alumina–15 vol% mullite composites during the sintering. The nanopowders of alumina–mullite composite were synthesized by the sol–gel method using aluminum chloride hexahydrate and two different silicon sources (colloidal silica in route 1 and tetraethyl orthosilicate in route 2). The alumina–mullite composites were prepared by pressing and sintering of the nanopowders. Although the intergranular mullites were observed in both routes, there were mullite particles in route 2 formed inside the alumina grains (intragranular mullite). Formation of the intragranular mullite is attributed to the drop in silica solubility, which occurs during the transition from metastable alumina to stable alumina. Compared to route 1, the relative density and the average grain size were increased and accelerated by route 2. The two-stage sintering is not useful for the mullite decomposition.

Keywords Phase evolution · Microstructure development · Alumina · Mullite · Nanocomposite

A. Sedaghat · E. Taheri-Nassaj (✉)
Department of Materials Science and Engineering, Tarbiat Modares University, P.O. Box 14115-143, Tehran, Iran
e-mail: taheri@modares.ac.ir

G. D. Soraru
Department of Materials Engineering and Industrial Technology, University of Trento, Via Mesiano 77, 38050 Trento, Italy

T. Ebadzadeh
Materials and Energy Research Centre, P.O. Box 14155-4777, Tehran, Iran

1 Introduction

Alumina has different applications such as insulating refractory linings of furnaces, seals, thermocouple wire protection and armors because of its specific physical and mechanical properties (high melting point and high strength) [1–3]. Mullite[1] ($3Al_2O_3 \cdot 2SiO_2$) is one of the most extensively studied crystalline phases in the $Al_2O_3 \cdot SiO_2$ binary system [5, 6] due to its low thermal expansion, good thermal and chemical stability and high creep resistance [7]. Mullite in the alumina matrix reduces the Young's modulus and the thermal expansion coefficient of composite, leading to a better thermal shock resistance [8–10]. Meanwhile, mullite has low toughness and hardness [11]. Small mullite additions (5–15 vol%) allow desirable values of hardness and toughness of alumina to be maintained while reducing the Young's modulus below that of alumina, so that it is expected that the thermal shock behavior will be improved [12].

A number of recent works involved the addition of impurities in order to achieve better densification behavior and, as a consequence, higher densities and better microstructural and mechanical properties [13, 14]. Schehl et al. [15] presented a modified processing route, which consisted in the doping of a commercial high-purity alumina powder. So that its microstructure was modified with such nanoparticles as zirconia and mullite, formed at the sintering stage. As a result, the grain boundaries of high-purity alumina powder were modified

---

[1] Orthorhombic [4]. a = 7.54 ± 0.03 Å; b = 7.693 ± 0.03 Å; c = 2.890 ± 0.01.

by segregation of the secondary phases or by the formation of well-distributed zirconia and mullite nanoparticles. Thus it is possible to tailor the microstructures by means of secondary phases through referring to the corresponding phase equilibrium diagrams.

Very high homogeneous multicomponent ceramics and composite ceramics can be obtained via sol–gel method, for its energy and, therefore, synthesis temperature is low [16].

In this work, the alumina composite nanopowders were synthesized by sol–gel method using aluminum chloride hexahydrate and two different silicon sources. Then the alumina–mullite composites were prepared by pressing and sintering of the above nanopowders. The purpose of this work is a comparative study of microstructural development in the sol–gel derived alumina–mullite nanocomposites.

2 Experimental

As shown in Fig. 1, the alumina composite nanopowders were synthesized using aluminum chloride hexahydrate[2] (dissolved in distilled water) and two different silicon sources (colloidal silica[3] in route 1 and tetraethyl orthosilicate[4] (TEOS) in route 2). The absolute ethanol was used as homogenizing agent for TEOS. According to the stoichiometric ratio of mullite ($3Al_2O_3 \cdot 2SiO_2$) and the desired volume percentage (15 vol%) of mullite, the aqueous solution of aluminum chloride hexahydrate and the required amount of colloidal silica (in route 1) or the alcoholic solution of TEOS (in route 2) were refluxed at 60 °C for 24 h. Also a mullite gel was prepared using the aqueous solution of aluminum chloride hexahydrate and the alcoholic solution of TEOS (in route 2). After condensation, the gels were dried at 120 °C for 24 h and ground in an agate mortar. The precursors of alumina–mullite composites were calcined at 900 °C for 2 h. The calcined powders were ball milled using alumina balls and absolute ethanol. After drying, the powders were sieved using a 80 μm mesh. The mullite gel was calcined at different temperatures for 2 h.

Figure 2 shows the transmission electron microscopy (TEM) images of the synthesized nanopowders by two routes. The properties of these nanopowders are summa-
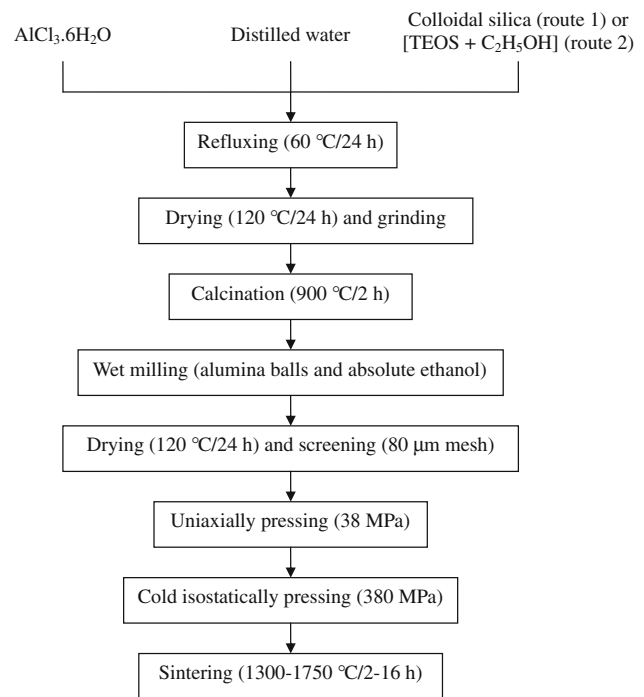
Fig. 1 The flow chart of processing of alumina–mullite nanocomposite with two different silicon sources, route 1 colloidal silica, route 2 TEOS

rized in Table 1. Nitrogen adsorption/desorption analysis was performed at −195 °C on ASAP2010 Micrometrics. The apparent density of the nanopowders, was measured using a helium picnometer (Micromeritics 1035).

The powders were uniaxially pressed under 38 MPa. Then they were cold isostatically pressed (CIP) at 380 MPa and, finally, sintered in air at 1,300, 1,500, 1,650 and 1,750 °C for 2 h. Also some samples of route 1 were randomly sinter and at 1,650 °C for 8 and 16 h.

X-ray diffraction (XRD) was carried out in the range of $10 < 2\theta < 80$ using Philips X-pert model with Cu Kα radiation. The microstructures of sintered bodies were studied by a XL 30, field emission environmental scanning electron microscope (FE-SEM) equipped with a link energy dispersive X-ray system. The specimens for SEM were polished to a 1 μm surface finish using diamond spray. Thereafter, they were thermally etched for 1 h at 100 °C below the sintering temperature. The grain size distributions on the polished samples were measured by using image analysis software (ImageJ 1.40 g).

The Archimedes method [17] was used to measure the density of the samples sintered by distilled water as an immersion medium and determine three mass values (dry, suspended and saturated masses). Moreover, the relative density was calculated by dividing the bulk density to the theoretical density of the specimen.
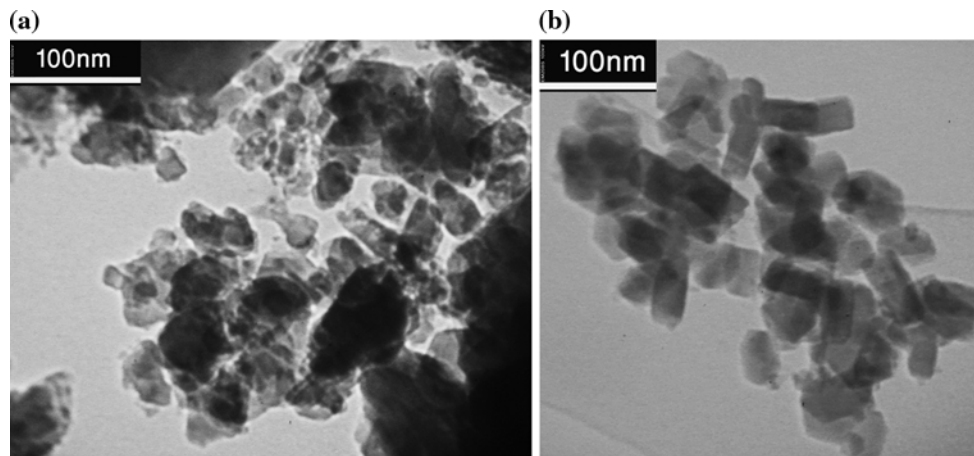
Fig. 2 **a** The TEM micrographs (bright field) of alumina–15 vol% mullite precursor calcined at 900 °C for 2 h: **a** by route 1 (average particle size 34 nm), **b** by route 2 (average particle size 31 nm)

Table 1 Properties of the alumina–15 vol% mullite precursors calcined at 900 °C for 2 h

	Route 1	Route 2
BET surface area (m^2/g)	105.4 ± 0.4	120.9 ± 0.5
Apparent density (g/cm^3)	3.646 ± 0.007	3.637 ± 0.003
Surface area of pores (m^2/g)	106	123
Total pore volume (cm^3/g)	0.50	0.51
Average pore diameter (nm)	19.0	17.0

3 Results and discussion

Figure 3 presents the XRD patterns of the alumina–15 vol% mullite precursors calcined at different temperatures (900–1,750 °C) by route 1. It also shows the transitional alumina (γ [18], κ [19]) at 900 °C. The crystallization of quartz [20] and tridymite [21] can be observed at 1,000 °C. Since silica retards the phase transformation of transitional alumina to alpha alumina [22], only some of the transitional alumina has been transformed to alpha alumina.

At higher temperatures (1,300–1,650 °C), the peaks of mullite [23] were detected (Fig. 3), while at 1,750 °C, the peaks of mullite were too weak and the alpha alumina peaks [24] were observed in both of the routes 1 and 2. The stability range of mullite is limited by a variety of thermal decomposition reaction schemes in time–temperature–P_{total}–P_{H2O} space [25, 26]. In another work, after annealing of mullite at 1,400 °C/4 h in dry air at normal pressure, thermal decomposition of mullite gave rise to the simultaneous formation of α-alumina platelets and an initially siliceous glassy phase completely wetting the platelets [27]. Meanwhile, mullite specimen surfaces heat-treated in helium between 1,650 and 1,800 °C degrade with

the formation of alpha alumina and volatile silicon species so that the recession progresses from the surface towards the bulk of the specimens [28]. So it can be concluded in our samples, that the mullite was decomposed.

Figure 4 shows the densification of alumina–15 vol% mullite composites after being sintered at 1,300, 1,500, 1,650 and 1,750 °C for 2 h by the routes 1 and 2. After sintering, the relative density of the samples increased by increasing of the temperature. In route 1, the relative densities were calculated as 49.8 ± 0.3, 75.9 ± 0.7 and 96.1 ± 0.5% T.D. at 1,500, 1,650 and 1,750 °C, respectively. So full densification could be obtained by increasing of the temperature in this route, but the mullite decomposition was observed at 1,750 °C (Fig. 3). At 1,500, 1,650 and 1,750 °C, the relative densities of route 2 were obtained as 67.2 ± 0.3, 99.2 ± 0.6 and 99.3 ± 0.7% T.D., respectively. Compared to route 1, the relative density was increased and accelerated by route 2. On the other hand, the BET surface areas of the nanopowders synthesized by routes 1 and 2 were 105.4 ± 0.4 and 120.9 ± 0.5 m^2/g, respectively. So the densification was improved in route 2, because the BET surface area of the nanopowder, synthesized by this route, was more than that in route 1. At 1,500 °C, the densification was not completed and at 1,750 °C, the mullite was decomposed according to its XRD pattern. Then in route 1, it was preferred to sinter it at 1,650 °C.

The microstructures of the sintered alumina–mullite composite obtained in route 1 at 1,500, 1,650 and 1,750 °C are shown in Fig. 5a, b and c, respectively. As shown, the average grain size increases by increasing of the temperature, so that it is 0.2, 0.4 and 0.9 μm at 1,500, 1,650 and 1,750 °C, respectively. These micrographs were taken in back-scattered electrons (BSE) mode of FE-SEM to
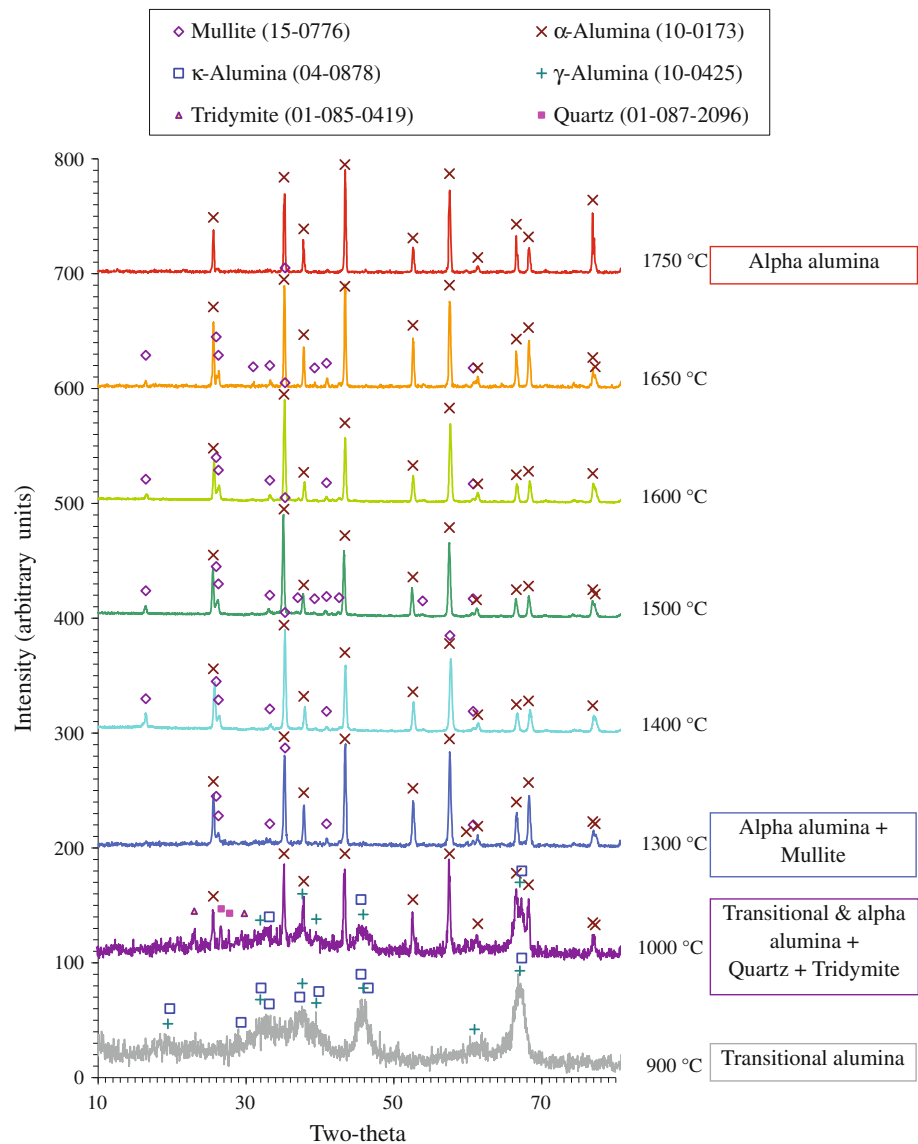
investigate the mullite phase. There are dark and light areas in the micrographs. Because of the energy-dispersive X-ray spectroscopy (EDS) spectrum of these areas (Fig. 5b) and their XRD patterns (Fig. 3), the mullite grains were formed between the alumina grains (intergranular mullite). At 1,750 °C (Fig. 5c), porosity was observed due to sintering (abnormal grain growth) or mullite decomposition.

The microstructures of the sintered alumina–mullite composite obtained by route 2 at 1,500, 1,650 and 1,750 °C are shown in Fig. 6a, b and c, respectively. It is observed that the average grain size increases by increasing of the temperature, so that it is 0.4, 1.4 and 2.2 μm at 1,500, 1,650 and 1,750 °C, respectively. Compared to route 1, the average grain size was increased and accelerated in route 2. These micrographs were taken in BSE mode of FE-SEM to investigate the mullite phase. There are dark and light areas in the micrographs. Because of the EDS spectrum of these areas (Fig. 6b) and their XRD patterns, the mullite particles were formed inside the alumina grains (intragranular mullite). At 1,750 °C (Fig. 6c), porosity was observed due to sintering (abnormal grain growth) or mullite decomposition.

The mullitization temperature in routes 1 and 2 was different. The former showed mullite formation at 1,300 °C, while the latter showed mullite formation by firing at around 1,000 °C (Fig. 7) due to the complete three-dimensional homogeneity, exemplified by the single-phase gel. Okada et al. [29] reported the mullitization temperature above 1,200 °C, using silica sol and aluminum salt. A molecular mullite gel can directly crystallize to the orthorhombic form of mullite (i.e., o–mullite, $3Al_2O_3 \cdot 2SiO_2$) [30].
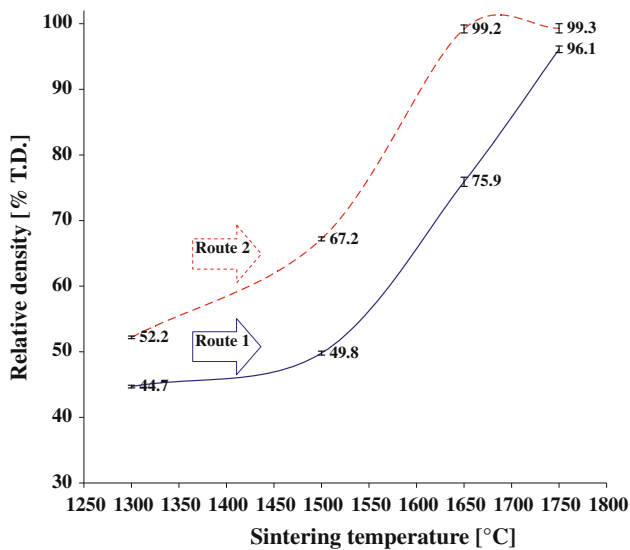
Fig. 4 The densification of alumina–15 vol% mullite composites after being sintered at 1,300–1,750 °C for 2 h

Boehmite (AlO(OH)) solid-solution gel, which yields stoichiometric mullite ($3Al_2O_3 \cdot 2SiO_2$) at high temperatures, was prepared by a hydrazine method using hydrous aluminum chloride and silicon ethoxide [31]. The sequence of phase development was summarized as follows: AlO(OH)(ss) gel → amorphous → γ-Al_2O_3(ss) → $3Al_2O_3 \cdot 2SiO_2$ [31]. So the metastable alumina phase has a solubility of silica. The difference in theoretical density of metastable and stable alumina phases (3.41 g/cm^3 for gamma alumina, as compared to 3.98 g/cm^3 for alpha alumina [32]) supports the solubility of silica. Also the complete three-dimensional homogeneity appears to support it in the route 2 of this work. As a consequence, the transition from metastable to stable alumina is likely to be associated with the formation of solute-rich precipitates. Based on the XRD analysis of route 2 (Fig. 7), it would be reasonable to imagine that precipitation of mullite is an inevitable outcome of the transition of alumina from gamma to alpha.
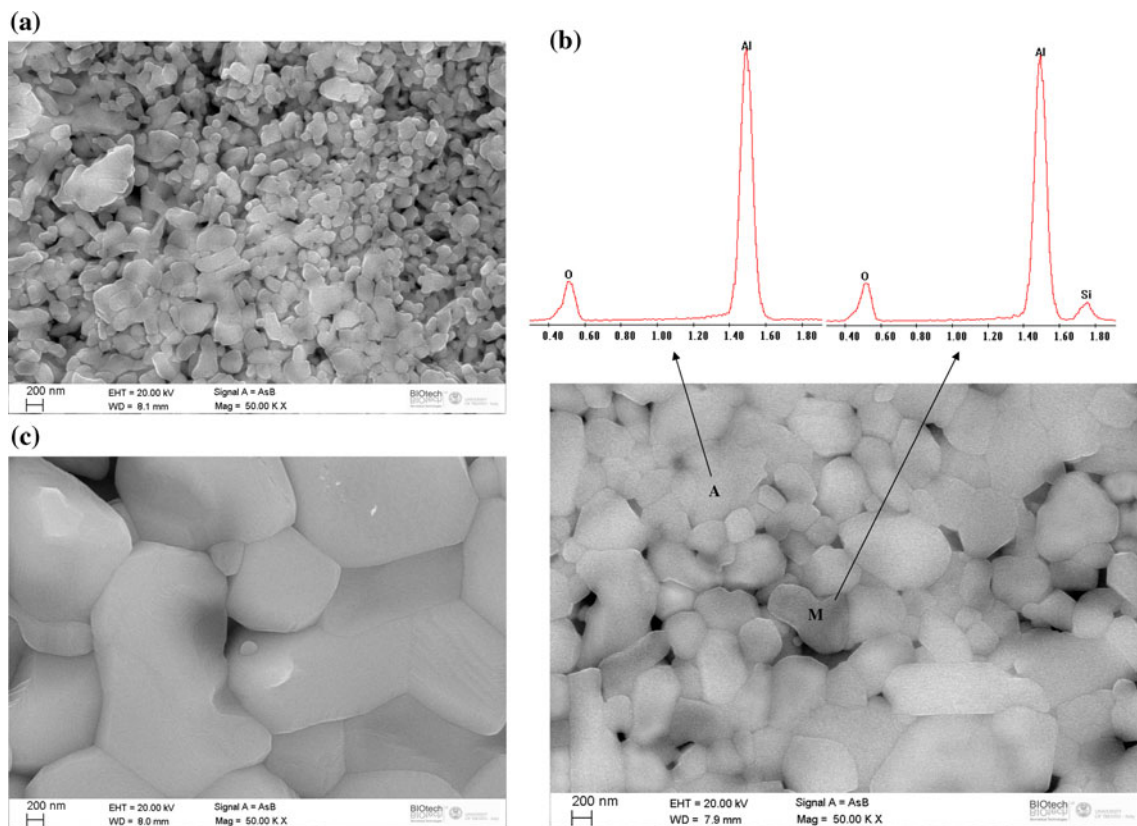

Fig. 5 The FE-SEM micrographs (BSE mode) of alumina–15 vol% mullite sintered at different temperatures for 2 h from route 1 and the EDS spectrum of points *A* and *M* (*A*: alumina, *M*: mullite) at 1,650 °C: **a** At 1,500 °C: 49.8% T.D., 0.2 μm average grain size. **b** At 1,650 °C: 75.9% T.D., 0.4 μm average grain size. **c** At 1,750 °C: 96.1% T.D., 0.9 μm average grain size
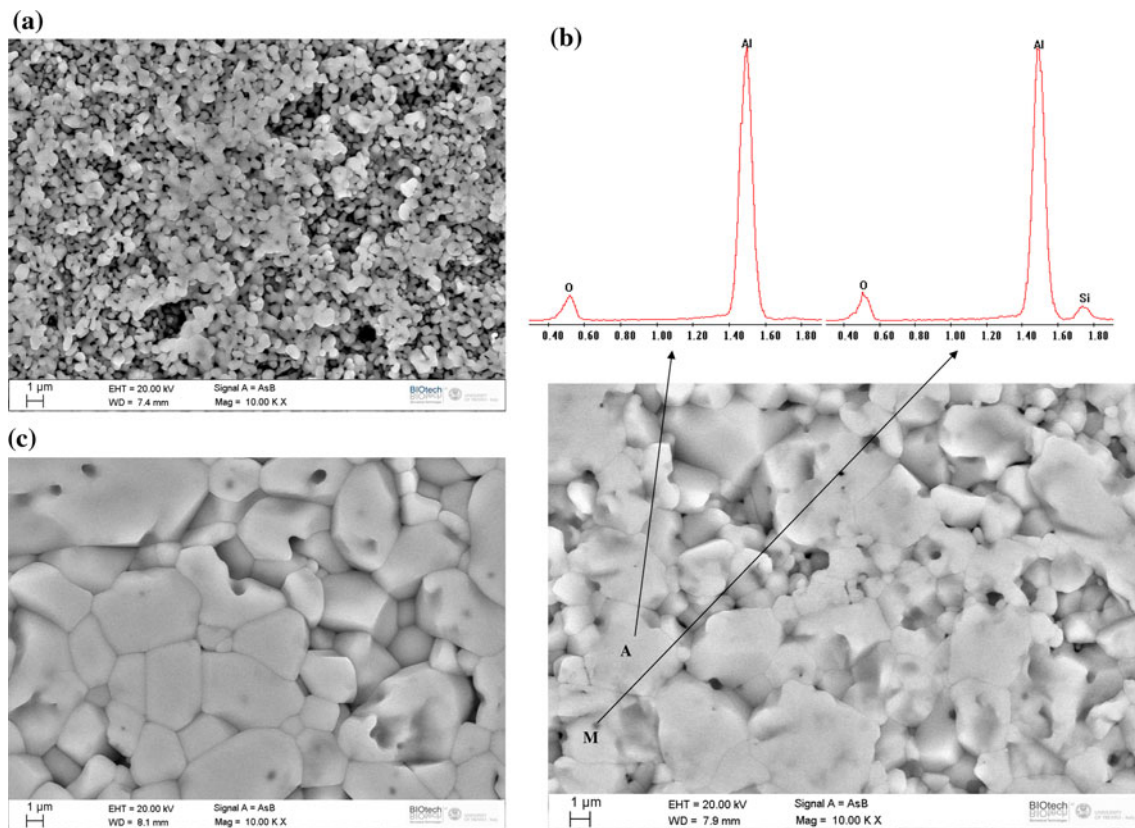
Fig. 6 The FE-SEM micrographs (BSE mode) of alumina–15 vol% mullite sintered at different temperatures for 2 h from route 2 and the EDS spectrum of points *A* and *M* (*A*: alumina, *M*: mullite) at 1,650 °C: **a** At 1,500 °C: 67.2% T.D., 0.4 μm average grain size. **b** At 1,650 °C: 99.2% T.D., 1.4 μm average grain size. **c** At 1,750 °C: 99.3% T.D., 2.2 μm average grain size

Katarína et al. [33] verified the applicability of two-stage sintering as a means of suppressing the final stage grain growth of submicrometer alumina. The first heating step should be short at a relatively high-temperature in order to close porosity without significant grain growth. The second step at lower temperature facilitates further densification with limited grain growth. Li and Ye [34] reported that below 82% T.D., alumina nanopowder would not be densified even after prolong soaking in the second step. Figure 4 shows that the relative density of alumina–15 vol% mullite is 75% T.D. at 1,650 °C. On the other hand, Fig. 8 shows the XRD patterns of this sample after being sintered at 1,650 °C for 2, 8 and 16 h. Instead of the mullite, tridymite and quartz phases were detected at 8 and 16 h. So the two-stage sintering is not suggested for sintering because of the mullite decomposition. However, the application of two-stage sintering for alumina is questionable, because according to Kanters et al. [35], the activation energy of densification in alumina is in fact higher than the activation energy of grain growth.

4 Conclusions

In this work, the alumina composite nanopowders, synthesized via sol–gel method using aluminum chloride hexahydrate and two different silicon sources (route 1: colloidal silica, route 2: TEOS), were used to prepare the alumina–mullite composite by pressing and sintering. The findings can be summarized as follows:

1. In route 1, the mullite grains were formed between the alumina grains (intergranular mullite), while in route 2, there were mullite particles formed inside the alumina grains (intragranular mullite).
2. Formation of intragranular mullite was attributed to the drop in silica solubility, which occurred during the transition from metastable alumina (exhibiting silica solubility) to stable alumina (with no silica solubility).
3. Compared to route 1, the relative density and the average grain size were increased and accelerated by route 2.
4. The two-stage sintering is not suggested for sintering because of the mullite decomposition.

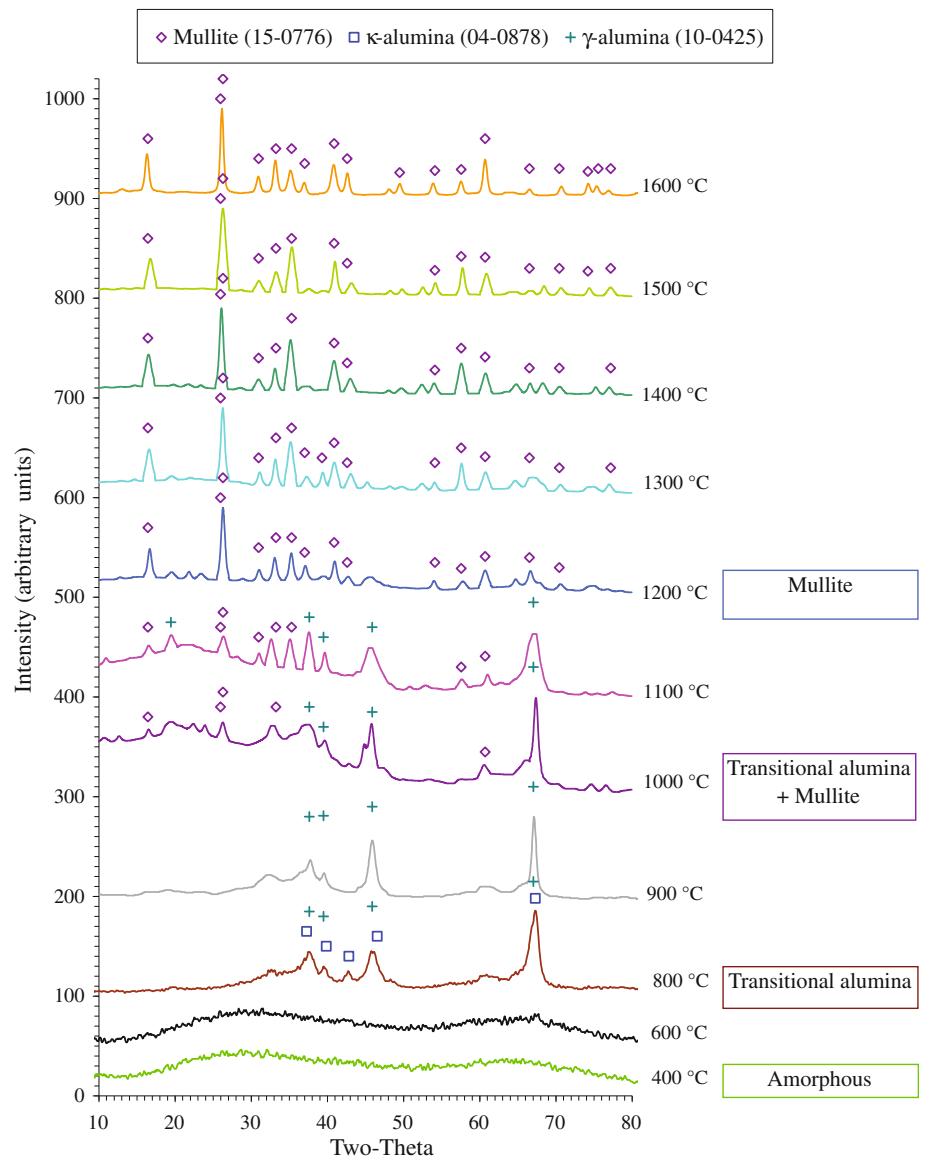**Fig. 7** The XRD patterns of mullite gel prepared by route 2 after being calcined at different temperatures
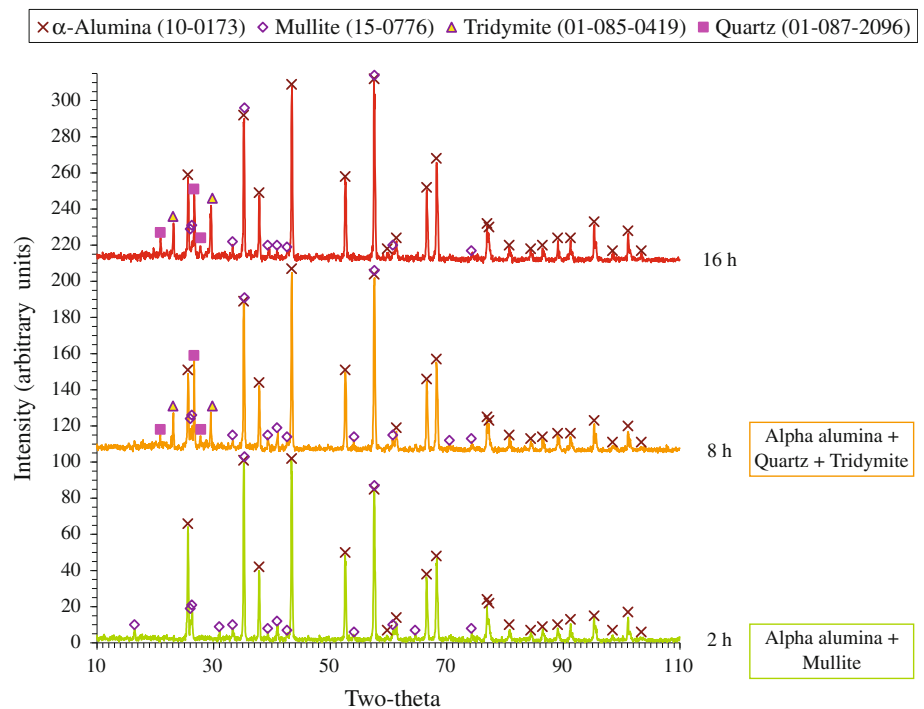
Fig. 8 The XRD patterns of alumina–15 vol% mullite composite from route 1 after being sintered at 1,650 °C for 2, 8, 16 h

References

1. Richerson DW (1992) Modern ceramic engineering. Marcel Dekker, New York, pp 808–823
2. Medvedovski E (2006) Alumina–mullite ceramics for structural applications. Ceram Int 32:369–375
3. Luo HH, Zhang FC, Roberts SG (2008) Wear resistance of reaction sintered alumina/mullite composites. Mat Sci Eng A 478:270–275
4. Shackelford JF, Alexander W (2001) Materials science and engineering handbook. CRC Press LLC, USA
5. Davis RF, Pask JA (1972) Diffusion and reaction studies in the system Al_2O_3–SiO_2. J Am Ceram Soc 55:525–531
6. Aksaf IA, Pask JA (1975) Stable and metastable equilibria in the system SiO_2–Al_2O_3. J Am Ceram Soc 58:507–512
7. Aksay IA, Dabbs DM, Sarikaya M (1991) Mullite for structural, electronic, and optical applications. J Am Ceram Soc 74:2343–2358
8. Mezquita S, Uribe R, Moreno R, Baudín C (2001) Influence of mullite additions on thermal shock resistance of dense alumina materials, Part 2: Thermal properties and thermal shock behaviour. Br Ceram Trans 100(6):246–250
9. Aksel C (2003) The effect of mullite on the mechanical properties and thermal shock behaviour of alumina–mullite refractory materials. Ceram Int 29:183–188
10. Zhang FC, Luo HH, Roberts SG (2007) Mechanical properties and microstructure of Al_2O_3/mullite composite. J Mater Sci 42:6798–6802
11. Aksel C (2002) The role of fine alumina and mullite particles on the thermomechanical behaviour of alumina–mullite refractory materials. Mater Lett 57:708–714
12. Moreno R, Mezquita S, Baudín C (2001) Influence of mullite additions on thermal shock resistance of dense alumina materials, Part 1: Processing studies. Br Ceram Trans 100(6):241–245
13. Thompson AM, Soni KK, Chan HM, Harmer MP, Williams DB, Chabala JM, Levi-Scotti R (1997) Dopant distributions in rare-earth-doped alumina. J Am Ceram Soc 80(2):373–376
14. Fang J, Thompson AM, Harmer MP, Chan HM (1997) Effect of yttrium and lanthanum on the final-stage sintering behavior of ultrahigh-purity alumina. J Am Ceram Soc 80(8):2005–2012
15. Schehl M, Díaz LA, Torrecilla R (2002) Alumina nanocomposites from powder-alkoxide mixtures. Acta Mater 50:1125–1139
16. Won CW, Siffert B (1998) Preparation by sol–gel method of SiO_2 and mullite ($3Al_2O_3·2SiO_2$) powders and study of their surface characteristics by inverse gas chromatography and zetametry. Colloid Surf A Physicochem Eng Asp 131:161–172
17. Standard Test Method for Water Absorption, Bulk Density, Apparent Porosity, and Apparent Specific Gravity of Fired Whiteware Products, ASTM Designation (2005) :C 373–388, ASTM standards, vol. 15.02
18. Powder Diffraction File, Card No. 10-0425, JCPDS
19. Powder Diffraction File, Card No. 04-0878, JCPDS
20. Powder Diffraction File, Card No. 01-087-2096, JCPDS
21. Powder Diffraction File, Card No. 01-085-0419, JCPDS
22. Sedaghat A, Taheri-Nassaj E, Naghizadeh R (2006) An alumina mat with a nano microstructure prepared by centrifugal spinning method. J Non-cryst Solids 352:2818–2828
23. Powder Diffraction File, Card No. 15-0776, JCPDS
24. Powder Diffraction File, Card No. 10-0173, JCPDS
25. Jacobson NS (1993) Corrosion of silicon-based ceramics in combustion environments. J Am Ceram Soc 76(1):3–28
26. Opila EJ (2003) Oxidation and volatilization of silica formers in water vapor. J Am Ceram Soc 86(8):1238–1248
27. Hildmann B, Braue W, Schneider H (2008) Topotactic growth of α-alumina platelets on 2/1 mullite single crystal surfaces upon thermal decomposition of mullite in dry and wet atmospheres. J Eur Ceram Soc 28:407–423
28. Schneider H, Komarneni S (2005) Mullite. WILEY-VCH Verlag GmbH & Co. KGaA, Weinheim, pp 236–237
29. Okada K, Otsuka N, Sh Somiya (1991) Review of mullite synthesis routes in Japan. Am Ceram Soc Bull 70(10):1633–1640
30. Huling JF, Messing GL (1992) Chemistry-crystallization relations in molecular mullite gels. J Non-Cryst Solids 147,148:213–221

31. Imose M, Takano Y, Yoshinaka M, Hirota K, Yamaguchi O (1998) Novel synthesis of mullite powder with high surface area. J Am Ceram Soc 81(6):1537–1540

32. Bowen P, Carry C, Luxembourg D, Hofmann H (2005) Colloidal processing and sintering of nanosized transition aluminas. Powder Technol 157:100–107

33. Bodišová K, Šajgalík P, Galusek D, Švančárek P (2007) Two-stage sintering of alumina with submicrometer grain size. J Am Ceram Soc 90(1):330–332

34. Li J, Ye Y (2006) Densification and grain growth of Al_2O_3 nanoceramics during pressureless sintering. J Am Ceram Soc 89(1):139–143

35. Kanters J, Eisele U, Rödel J (2000) Effect of initial grain size on sintering trajectories. Acta Mater 48:1239–1246